The Dependence of Spike Field Coherence on Expected Intensity

Kyle Q. Lepage
lepage@math.bu.edu
Mark A. Kramer
mak@bu.edu
Uri T. Eden
tzvi@math.bu.edu
Department of Mathematics and Statistics, Boston University, Boston,
MA 15213, U.S.A.

The coherence between neural spike trains and local-field potential recordings, called spike-field coherence, is of key importance in many neuroscience studies. In this work, aside from questions of estimator performance, we demonstrate that theoretical spike-field coherence for a broad class of spiking models depends on the expected rate of spiking. This rate dependence confounds the phase locking of spike events to field-potential oscillations with overall neuron activity and is demonstrated analytically, for a large class of stochastic models, and in simulation. Finally, the relationship between the spike-field coherence and the intensity field coherence is detailed analytically. This latter quantity is independent of neuron firing rate and, under commonly found conditions, is proportional to the probability that a neuron spikes at a specific phase of field oscillation. Hence, intensity field coherence is a rate-independent measure and a candidate on which to base the appropriate statistical inference of spike field synchrony.

1 Introduction

Neural activity coupled between spatially disparate regions is thought to play a vital role in brain function (Buzsaki & Draguhn, 2004; Singer & Gray, 1995) and disease (Ben-Ari, 2007). Many measures exist to characterize this coupling: traditional measures of linear association, such as cross-correlation, measures of nonlinear relationships (Pereda, Quiroga, & Bhattacharya, 1995), and measures of cross-frequency coupling (Canolty et al., 2006). A coupling measure commonly estimated when analyzing neuroscientific data is the coherence—a frequency domain measure used to assess the phase relationship between two oscillatory signals (Bruns, 2004; Priestly, 1981). In neuroscience, coherence measures are typically estimated from field recordings, for example, the estimates of coherence between two

electroencephalogram (EEG) signals or fields (Bullock et al., 1995; Nunez et al., 1997), between two electrocorticogram (ECoG) signals (Towle, Carder, Khorasani, & Lindberg, 1999; Zaveri et al., 1999), or between two local field potential (LFP) signals (Buzsaki, Horváth, Urioste, Hetke, & Wise, 1992; Montgomery & Buzsáki, 2007). In these cases, the "field-field" coherence is independent of the field amplitude; scaling observations of one field by a constant amount does not affect its coherence with another field.

Coherence may also be estimated to assess the relationship between neural spike trains and fields (Jarvis & Mitra, 2001). This spike field coherence is of key importance in many neuroscience studies as a measure of consistent neural spiking at a specific phase of the field, usually an LFP (Fries, Womelsdorf, Oostenveld, & Desimone, 2008; Gregoriou, Gotts, Zhou, & Desimone, 2009; Pesaran, Pezaris, Sahani, Mitra, & Andersen, 2002; Pesaran, Nelson, & Andersen, 2008). In this letter, we show that the spike field coherence measure reflects features of the mean firing rate, as well as features of the relationship between spiking activity and the phase of field.[1] As preliminary intuition for this result, note that two sources of variability affect neural spiking: variations in rate and variability due to the randomness of spiking events. That is, even for a constant known rate, randomness remains in the spiking activity due to the random appearance of the spikes. More generally, each source of variation, both the random rate and the random spike times, contributes, and thus the coherence between spikes and fields is more complicated than that between two fields.

While coherence remains a useful measure of characterizing relationships between neural spiking activity and fields, it is important that researchers remain aware of the effect of neural firing rate on the coherence. In this work, the statistical performance of spike field coherence estimators is not investigated. Instead, we demonstrate that theoretical spike field coherence for a broad class of spiking models depends on the expected rate of spiking. Bias is not the concern here; the dependence on rate relates to fundamental aspects of the spike field coherence measure. Further, this class of models, a subset of the class of doubly stochastic discrete-time point processes, is shown to exhibit spiking behavior similar to actual spiking data, hence providing a foundation for inference.

The letter begins with background on coherence in section 2; states the main result of the letter, the dependence of spike field coherence on rate, in sections 3, and illustrates this dependence by simulation in section 4. In section 5, we provide important but secondary results. Section 6 consists of the mathematical development of the results presented in sections 3 and 5. The letter concludes with a discussion in section 7.

---

[1] Here, for the sake of pedagogy, *rate* is used colloquially to mean the number of spikes divided by the duration observed. In section 6, where results are presented with mathematical accuracy, the conditional intensity replaces this informal notion of rate.

2 Background

Coherence is a frequency-dependent measure of linear association between two time series. Nonparametric coherence estimators are common and have been successfully employed in diverse sciences. Coherence, for example, plays a role in optics (Mandel & Wolf, 1995; Schmitt, 1999) and in geophysics (Foster & Guinzy, 1967; Hinich & Clay, 1968; Munk & Phillips, 1968). In neuroscience, background material on field-field coherence and spike field coherence includes Amjad, Halliday, Rosenberg, and Conway (1997), Brillinger (2001), Halliday, Rosenberg, Amjad, Breeze, Conway, and Farmer (1995), Jarvis and Mitra (2001), Mitra and Bokil (2008), Rosenberg, Halliday, Breeze, and Conway (1998). Coherence in the neuroscience setting has been used to characterize neural population activity (Bollimunta, Chen, Schroeder, & Ding, 2008; Bruns & Eckhorn, 2004; Bullock et al., 1995; DeCoteau et al., 2007a, 2007b; Kristeva, Patino, & Omlor, 2007; Montgomery & Buzsáki, 2007; Sirota et al., 2008; Towle et al., 1999; Zaveri et al., 1999), and the relationship between neural spiking and field potentials (Chalk, Herrero, Gieselmann, Delicato, Gotthardt, & Thiele, 2010; Fries, Reynolds, Rorie, & Desimone, 2001; Fries et al., 2008; Gregoriou et al., 2009; Jutras, Fries, & Buffalo, 2009; Pesaran et al., 2008; Witham, Wang, & Baker, 2007; Womelsdorf, Fries, Mitra, & Desimone, 2006). Coherence can be estimated between any two time series, providing information about phase relationships, group delays, and transfer functions, in addition to the degree of linear interdependence (Brillinger, 2001; Priestly, 1981). For a multitaper estimator of coherence see Thomson (1982), and for the robust estimation of these quantities see Chave, Thomson, and Ander, 1987. Multivariate extensions of coherence (i.e. canonical coherence) are discussed in, for example, Brillinger (2001) and applied in a neuroscience context in Brillinger, Lindsay, and Rosenberg (2009). Coherence analysis is a component of the spectral analysis of time series. Related work on the spectral analysis of point processes includes Bartlett (1963, 1981), Brillinger et al. (2009), and Jarvis and Mitra (2001).

Any stochastic model describing the relation between two time series implicitly defines a theoretical coherence between them as well. As is typical in spectral analysis approaches, in this work neural signals of interest (LFPs and spike trains) are assumed weak-sense stationary (Priestly, 1981). This implies that the mean and covariance of these signals do not vary in time. It is important to note that in many electrophysiological studies, the recorded signals will not satisfy this assumption. For example, many experiments involve presenting predetermined, dynamic stimuli that lead to response properties that vary in time. However, in these cases, it is often possible to meaningfully proceed with spectral analysis despite the stationary restriction. This can be done by either identifying short time intervals over which neural responses are approximately weak-sense stationary or by quantifying the performance of spectral estimators when the weak-sense stationary assumption is inappropriate.

To define coherence, let x_t be a mean-zero, discrete-time, weak-sense stationary random process modeling one of two time series. Let y_t be another mean-zero, discrete-time, weak-sense stationary random process modeling the other time series. Further define the discrete Fourier transforms, $X_T(f)$ and $Y_T(f)$, as

$$X_T(f) = \frac{\Delta}{T} \sum_{t=0}^{N-1} x_t e^{-i2\pi f t \Delta} \tag{2.1}$$

and

$$Y_T(f) = \frac{\Delta}{T} \sum_{t=0}^{N-1} y_t e^{-i2\pi f t \Delta}, \tag{2.2}$$

where $T = N\Delta$ is the duration of the time series, Δ is the time between consecutive measurements, and $i^2 = -1$. Here t is the integer valued time index such that the corresponding measurement time is $t\Delta$. Note that in the frequency domain, quantities will be continuous functions of the frequency, f. This is a property of the discrete Fourier transform (Oppenheim & Schafer, 2009). Then the coherence, $C_{xy}(f)$, between x_t and y_t, is[2]

$$C_{xy}(f) = \lim_{T \to \infty} \frac{E\left[X_T(f) Y_T^*(f)\right]}{\sqrt{E\left[\left|X_T(f)\right|^2\right] E\left[\left|Y_T(f)\right|^2\right]}}, \tag{2.3}$$

where E denotes the expectation operator (Percival & Walden, 1993) and is the average over realizations (i.e., average across trials). Some properties of this measure include the following. First, by the Cauchy-Schwartz inequality, $0 \le \left|C_{xy}(f)\right| \le 1$. Second, the magnitude of the coherence, $\left|C_{xy}(f)\right| = 1$ when $X_T(f) = k\,Y_T(f)$ for $k \in \mathbb{C}$. This latter relationship arises from the fact that equality in the Cauchy-Schwartz inequality is achieved when there is a linear relationship between $X_T(f)$ and $Y_T(f)$. Hence, $\left|C_{xy}(f)\right|$ provides a per frequency indication of linear association between the time series x_t and y_t. Though not focused on in this work, the phase of $C_{xy}(f)$ provides information regarding the timing of x_t with respect to y_t at the frequency f. An estimate of the coherence plays a role in standard nonparametric

---

[2]Term *coherence* is sometimes reserved for the magnitude of the complex quantity specified in equation 2.3. In Priestly (1981), for instance, $C_{xy}(f)$ is called "complex coherency," or just "coherency," and *coherence* is reserved for $\left|C_{xy}(f)\right|$. In this letter, $C_{xy}(f)$ will be called the coherence, and when referring to magnitude and magnitude squared quantities, explicit reference will be made.

estimates of the transfer function between the time series x_t and y_t.[3] It embodies information, at the frequency f, regarding both the amplitude scaling between the two time series, in addition to the difference in phase between the time series (Priestly, 1981; Thomson, 1982).

When the cross-covariance and autocovariance sequences between the pair-wise combinations of x_t and y_t exist, Wold's theorem guarantees the existence of the corresponding integrated spectra (Priestly, 1981). When the relevant integrated spectra are differentiable, the spectrum of x_t, y_t, and their cross-spectrum ($S_{xx}(f)$, $S_{yy}(f)$, and $S_{xy}(f)$, respectively) exist, and the coherence, $C_{xy}(f)$, can be expressed as

$$C_{xy}(f) = \frac{S_{xy}(f)}{\sqrt{S_{xx}(f)S_{yy}(f)}}. \tag{2.4}$$

For neuroscience data, the existence and differentiability of the integrated spectra is, for all practical purposes, guaranteed, and equation 2.4 can be considered valid.

3 Result

The main result of this letter is the dependence of spike field coherence on the overall rate, or intensity, of spiking. The spike field coherence, $C_{ny}(f)$, can be defined in a fashion analogous to the definition of the field-field coherence, $C_{xy}(f)$, presented in section 2 but with important differences that account for the binary nature of the spike events. A brief outline of the results is presented here; readers interested in mathematical details are directed to section 6, where stochastic models are posited and the results are developed and discussed with greater precision. In the following, the term rate is used colloquially to mean the expected number of spikes in a given duration.

Consider a weak-sense stationary binary time-series model of random spiking activity with some rate, λ_t, that evolves in time and has mean μ_λ. In section 6, the spike field coherence is shown to be related to the rate field coherence,

$$C_{ny}(f) = C_{\lambda y}(f) \left(1 + \frac{\mu_\lambda + H(f)}{S_{\lambda\lambda}(f)}\right)^{-\frac{1}{2}}, \tag{3.1}$$

where $C_{\lambda y}(f)$ is the coherence between the rate and the field potential, $S_{\lambda\lambda}(f)$ is the spectrum of the rate, λ_t, and $H(f)$ is a parameter influenced by

---

[3]In the Fourier domain, the output of a linear, time invariant system can be represented as the multiplication of a "transfer function" with the Fourier transform of the input (Oppenheim & Schafer, 2009).

history-dependent spiking (such as a refractory period or periods of bursting). The behavior of this parameter is discussed heuristically in section 5.4 and is further discussed in section 6 for different types of neural activity. In particular, it is shown to be 0 for spiking activity without history dependence. Thus, the spike field coherence, $C_{ny}(f)$, depends on the two fields λ_t and y_t and the mean rate of neuron firing μ_λ.

To illustrate the dependence of the spike field coherence on the rate, consider a scaling of the rate λ_t of a Poisson process by a constant factor s. Doing so results in a scaled spectrum, $S_{\lambda\lambda}(f)$ multiplied by a factor proportional to s^2, accompanied by mean-rate μ_λ scaled by s. Thus, with increasing scaling, $\frac{\mu_\lambda}{S_{\lambda\lambda}(f)}$ tends to 0, and the spike field coherence tends to the rate field coherence $C_{\lambda y}(f)$. Because the probability of a spike about time index t is approximately $\Delta\lambda_t$, the rate field coherence provides a direct measure of the probability of spiking at a specific phase of an oscillation in the field y at frequency f. Hence, the rate field coherence is a natural measure of the association between spiking and field potential oscillations. With scaling tending to 0, $\frac{\mu_\lambda}{S_{\lambda\lambda}(f)} \to \infty$ and the spike field coherence tends to 0. In words, as the rate tends to 0, so does the spike field coherence. These results are demonstrated in simulation in section 4 and derived in detail in section 6.

4 Simulation

Two simulations are performed to illustrate the dependence of the spike field coherence, $C_{ny}(f)$, on mean rate. In the first, synthetic field potentials are generated from a stochastic field potential model, and synthetic spike trains are generated as realizations of two different types of point processes. For both types of point processes, the dependency between the field potentials and the time-varying spike rates remains constant, and for both types of point processes, realizations are generated for various mean spike rates. Thus, by varying the mean rates while maintaining a constant dependency between spike timing and field potential, the dependence of the coherence on the mean spike rate is explored.

The spike trains are realizations of one of two different types of point processes, with various mean spike rates. The first type of point process exhibits no history dependence in the spiking (e.g., no refractory period), but with spike rate depending on the phase of the field. The field is modeled simply as a second-order autoregressive random process. The spike rate depends on the exponentiated field, so that field increases manifest in increased rates. From these synthetic time series, coherences are estimated for different values of the mean-spiking rates using a standard software package .[4] These estimates are plotted for the frequency of maximal coherence

---

[4]Chronux Matlab Toolbox, freely available at www.chronux.org.
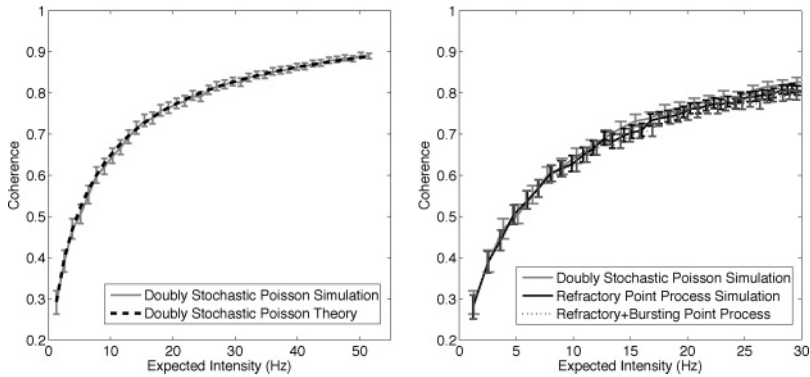
Figure 1: Simulated spike and field data illustrate the dependence of the spike field coherence on the mean spike rate. Multitaper estimates of the spike field coherence are estimated using the Chronux Matlab toolbox and compared to the magnitude of the theoretical spike field coherence, $|C_{ny}(f)|$, for a specific frequency as a function of the expected intensity or rate. This frequency, fixed as rate varies, is chosen such that the magnitude of the spike field coherence is maximal. (Left) Theoretical result from equation 3.1 plotted with the magnitude of the estimated spike field coherence. Theory lies within the 95% confidence interval specified by the gray error bars, and the dependence on rate is evident. (Right) An indication of the effect of history on the rate dependence of the magnitude of the spike field coherence. The magnitude of the spike field coherence is computed and plotted for three types of point processes. The first type (solid, light gray) has no history effect as in the left figure, the second contains a refractory period (solid, black), and the third type has bursting in addition to a refractory period (dotted). In these examples, the history effect does not appreciably alter the magnitude of the spike field coherence, and once again, the dependence on the rate of spiking is pronounced.

in Figure 1. The theoretical value of the magnitude of the spike field coherence, $C_{ny}(f)$, specified in equation 3.1, in the case of history-independent spiking, is also plotted in Figure 1 as a function of spike rate. This theoretical curve is well approximated by the magnitude of the spike field coherence estimates.

In the second type of point-process model, the spiking activity possesses two types of history dependence: one that enforces a refractory period (by decreasing the probability of spiking immediately after a spike) and another that, in addition to the refractory period, encourages bursting (by increasing the probability of spiking after the refractory period). In both cases, the spike rate still depends on the phase of the field model (simulated in the same way as above). For these more complicated situations, the dependence of the spike field coherence on the mean rate remains the same (see Figure 1, right). To summarize, in both model types, although the dependency

between the field and spiking activity remains unchanged, the spike field coherence decreases as the mean rate decreases.

A second illustration of the dependence of the spike field coherence, $C_{ny}(f)$, on the mean rate is provided by associating a true ECoG signal (recorded from human cortex during seizure) with simulated spiking data. This association is specified such that spiking activity is realized with two different overall rates—one high and one with a rate 10 times reduced. In both cases, the point processes are constructed so that spikes tend to occur at the peaks of the dominant 8 Hz field rhythm (see Figure 2, upper panel). Thus, the same association between the spiking and the field is maintained while the rate of firing is varied. The estimated magnitude of the spike field coherence for the high- and low-rate spiking are plotted in the bottom row of Figure 2. Ninety-five percent confidence regions are reported using the jacknife method for the large-coherence magnitude near 8 Hz. For either estimate of the spike field coherence, the maximum of the magnitude occurs at frequencies near 8 Hz by construction. The dependence of the spike field coherence on the rate is clear: the spike field coherence estimate computed from the high-rate spiking is greater than or equal to the magnitude of the spike field coherence estimate computed with the low-rate spiking. Though this simulation uses common estimates for the spike field coherence, one sees that this estimator demonstrates the dependence of the spike field coherence on the spiking rate expected from equation 3.1.

The simulation results presented in Figures 1 and 2 are unlikely if either the theoretical model is incorrect or if the standard multitaper spike field coherence estimator is badly biased.

5 Secondary Results

Additional results providing insight into the nature of spectral quantities of point processes are provided in this section. These results are developed in detail in section 6 and in the appendix. In the following, the collection of neuron spike times is represented as a realization of a discrete-time, doubly stochastic point process with increments, dn_t.

5.1 Autocovariance Function: Discrete-Time, Doubly Stochastic Point Process, $r_{nn}(t, \tau)$. In section A.3 in the appendix, we show that the spike-spike autocovariance sequence, in general a function of both a global time index, t, and a local time index, τ, is,

$$r_{nn}(t, \tau) + \Delta^2 \mu_{\lambda,t}\, \mu_{\lambda,t+\tau}$$

$$= \begin{cases} \Delta\, \mu_{\lambda,t}, & \tau = 0 \\ \Delta^2\, E_{\lambda_t,\lambda_{t+\tau}} \left[\lambda_t \lambda_{t+\tau} \frac{P(\lambda_{t+\tau}|\lambda_t, dn_t=1)}{P(\lambda_{t+\tau}|\lambda_t)} \right], & |\tau| > 0 \end{cases}. \tag{5.1}$$
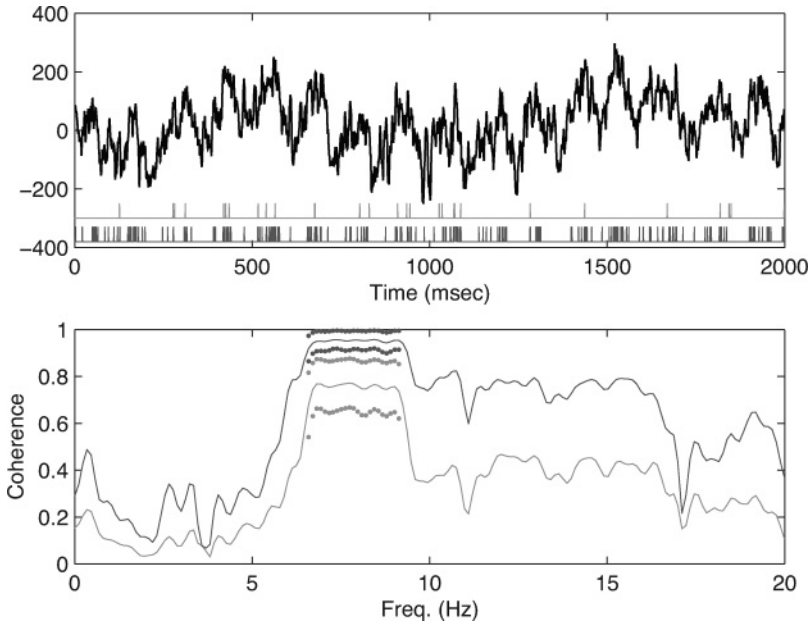
Figure 2: Illustration of rate dependence of the spike field coherence for experimental field data. (Top) Black curve: The neural signal to which neuron spiking is associated by simulation. An 8 Hz rhythm dominates this ECoG signal. Light gray raster plot indicates the low-firing-rate neuron spike times. Dark gray raster plot indicates the high-firing-rate neuron spike times. Note that the spike events tend to occur at the peaks of the 8 Hz rhythm in the field. (Bottom row) Light gray and dark gray curves: Magnitude of multitaper estimates of the spike field coherence, $C_{ny}(f)$, computed using the Chronux Matlab toolbox using default parameters. The resolution is approximately 2.5 Hz. The dotted curves near 8 Hz denote 95% jacknifed confidence intervals. The light gray curve is computed using the light gray neuron spike event times depicted in the light gray raster plot in the top row. The dark gray curve is computed using the dark gray neuron spike event times depicted in the dark gray raster plot in the top row. Note that the spiking process from which the dark gray and light gray spike events are drawn is constructed so that the rate field coherence, $C_{\lambda y}(f)$, has a magnitude near 1 for frequencies near 8 Hz. Further, note that the dark gray estimate of the spike field coherence magnitude, $|C_{ny}(f)|$, is larger than the light gray estimate for all frequencies and that the maximum of $|C_{ny}|$ occurs at a frequency of 8 Hz.

Here $\mu_{\lambda,t} = E[\lambda_t]$ is the mean intensity at time index t, the subscript under the expectation symbol denotes with respect to which variables the expectation is to be taken, and $P(\lambda_{t+\tau}|\lambda_t, dn_t = 1)$ is the probability density of the stochastic intensity at time index $t + \tau$ given the stochastic intensity at

time index t, in addition to knowledge that a spike occurred at time index t. When dn_t is weak-sense stationary and the discrete Fourier transform of $r_{nn}(t, \tau)$ with respect to τ exists, then the spectrum, $S_{nn}(f)$, of dn_t is equal to the discrete Fourier transform of $r_{nn}(t, \tau)$ with respect to τ. [5] Equation 5.1, valid for both stationary and nonstationary dn_t, describes the autocovariance structure of the spiking. The separate behavior of the autocovariance structure at $\tau = 0$ is not present for field-type processes and is due to the binary nature of the spiking. For $\tau \neq 0$, the autocovariance sequence generalizes from the expectation, $E\left[\lambda_t \lambda_{t+\tau}\right]$, in the case where there is no spiking dependence, to an expectation containing a ratio of probability densities depending on past spiking activity. These topics are elaborated on in section 6. A second expression for the spike-spike autocovariance, $r_{nn}(t, \tau)$, sheds further light on the autocovariance sequence, $r_{nn}(t, \tau)$:

$$r_{nn}(t, \tau) = \Delta^2 \mu_{\lambda,t} \, E\left[\lambda_{t+\tau} | dn_t = 1\right] - \Delta^2 \mu_{\lambda,t} \, \mu_{\lambda,t+\tau}. \tag{5.2}$$

Thus, the autocovariance sequence of dn_t depends on history only through the conditional expectation of $\lambda_{t+\tau}$. Further, for dn_t to be weak-sense stationary, both $\mu_{\lambda,t}$ and $E\left[\lambda_{t+\tau} | dn_t = 1\right]$ must be invariant with respect to changes in the time, t. More discussion is provided in section A.4.

5.2 Spike Field Cross-Spectrum, $S_{ny}(f)$. When the spike field cross-covariance function, $r_{ny}(t, \tau)$, does not depend on absolute time and is square integrable, the spike field cross-spectrum, $S_{ny}(f)$, is proportional to the intensity-field cross-spectrum, $S_{\lambda y}(f)$: [6]

$$S_{ny}(f) = \Delta S_{\lambda y}(f). \tag{5.3}$$

5.3 Spike-Spike Spectrum, $S_{nn}(f)$. When the spike time series, dn_t, is a realization of a weak-sense stationary, doubly stochastic, discrete-time point process, then, assuming the existence of the spectrum $S_{nn}(f)$, and the square integrability of the autocovariance function $r_{nn}(\tau)$, the spectrum can be approximated:

$$S_{nn}(f) \approx \Delta^2 \left(\mu_\lambda + H(f) + S_{\lambda\lambda}(f) \right). \tag{5.4}$$

Here, $S_{\lambda\lambda}(f)$ is the spectrum of the stochastic intensity, λ_t, and the mean intensity, $\mu_\lambda = E\left[\lambda_t\right]$, and $H(f)$ is a frequency-dependent term capturing the effect of history-dependent spiking. Note that the units of $S_{\lambda\lambda}(f)$ are in Hz^2 per Hz, and hence have units of Hz, as does μ_λ. In section 6, the development and accuracy of equation 5.4 are discussed.

---

[5]See Wold's theorem, presented in, for example, Priestly (1981).
[6]Assuming that the field, y_t, does not depend on past spikes.

5.4 The History-Dependent Factor, $H(f)$. The factor $H(f)$ affects both the spike field coherence, $C_{ny}(f)$, and the spike spectrum, $S_{nn}(f)$, and reflects history-dependent spiking effects, such as refractory periods. When dn_t is independent of $dn_{t'}$ for $t \neq t'$, $H(f)$ is equal to 0. When dn_t exhibits a refractory period of duration τ_r samples, $H(f)$ is equal to the intensity spectrum convolved with a Dirichlet-type kernel:

$$H(f) = -S_{\lambda\lambda}(f) * D_{\tau_r}(f) + o(\Delta). \tag{5.5}$$

The form of $D_{\tau_r}(f)$ and the derivation of equation 5.5 are provided in section 6.1.2 and A.5. Substituting equation 5.5 into equation 5.4, one obtains

$$S_{nn}(f) \approx \Delta^2 \left(\mu_\lambda + S_{\lambda\lambda}(f) * (\delta(f) - D_{\tau_r}(f)) \right). \tag{5.6}$$

Thus, the spike spectrum, $S_{nn}(f)$, is a shifted and scaled convolution of the intensity spectrum, $S_{\lambda\lambda}(f)$ with $\delta(f) - D_{\tau_r}(f)$, in the case of a refractory-type memory effect. The function, $D_{\tau_r}(f)$, has nonzero values over a range of frequencies, with energy concentrated for $|f| \lesssim \frac{1}{\tau_r}$ and a maximal value equal to τ_r at zero frequency. As described in section 6.1.2, when other history-dependent type effects are present in dn_t, the full expression for the spike spectrum, $S_{nn}(f)$ is

$$S_{nn}(f) = \Delta^2 \left(\mu_\lambda + S_{\lambda\lambda}(f) * (\delta(f) + G(f) * D_{\tau_{ro}}(f) - D_{\tau_r}(f)) \right), \tag{5.7}$$

where $G(f)$ is the discrete Fourier transform of the history-dependent function $g(\tau)$ defined in section 6.1.2 and $\tau_{ro} = \frac{\tau_o - \tau_r}{2}$ where τ_o is the delay beyond which a spike at time index t has a negligible influence on subsequent spiking.

6 Derivations

The spike field coherence, $C_{ny}(f)$, can be defined in a fashion analogous to the definition of the "field-field," or regular, coherence, $C_{xy}(f)$, presented in section 2. In analogy with a field-type time series, the number of spiking events that occur in the time interval $((t-1)\Delta, t\Delta)$ is a time series. Here, Δ is the time between field measurements introduced in section 2. It is advantageous to model this time series as a truncated realization of a discrete-time point process, dn_t. Here, dn_t is the number of spiking time events that occur in the interval $((t-1)\Delta), t\Delta)$, t integer, with Δ chosen

sufficiently small that the probability of multiple neuron firings within any span of time Δ is small. Specifically,

$$P(dn_t > 1) < O(\Delta^2). \tag{6.1}$$

Note that for single-neuron recordings, Δ can always be chosen sufficiently small, such that constraint 6.1 is satisfied, due to the refractory period suppressing subsequent neuron spiking in the time immediately following a neuron spike (Koch, 1999). A point process is completely characterized by its conditional intensity, λ_t,

$$\lambda_t = \lim_{\Delta \to 0} \frac{P\left(dn_t = 1 \mid H_t\right)}{\Delta}, \tag{6.2}$$

where H_t is the spike history process. Intuitively, the probability of an event at time index t equals $\Delta \cdot \lambda_t$, up to negligible corrections due to the small nonzero probability of multiple events in any one increment (Daley & Vere-Jones, 2003). In the situation where the increments, dn_t, conditioned on λ_t, do not depend on past increments, that is, on $dn_{t'}$ for $t' < t$, the point process is called Poisson, and the conditional intensity, λ_t, is equal to the rate of occurrence of spiking events. In this letter, reference to discrete-time Poisson processes is often made. Here the emphasis is on the independence property of Poisson processes, as the marginal probability mass function for dn_t for any sufficiently short interval is approximately a Bernoulli probability mass function. The discrete-time Poisson process model, while sometimes convenient, is physiologically inaccurate due to the fact that dependence on past spiking, such as the refractory period, is not modeled. Thus, to account for history-type spiking effects, the discrete-time Poisson process model is generalized to a discrete-time point-process model. An additional modeling difficulty arises in that actual neuron spiking exhibits a time-dependent probability of firing. In order to develop a spike field coherence in analogy with the regular coherence introduced in section 2, the first two moments of dn_t must be independent of absolute time. Time-dependent firing activity, while maintaining stationary mean and second moments can be attained by generalizing the discrete-time point process to a doubly stochastic discrete-time point process. That is, let the conditional intensity, λ_t, be itself a weak-sense stationary random process such that $\lambda_t \geq 0$. Therefore, the point-process modeling the spikes and the intensity, which determines the probability of a spike in each timestep, are both random processes. Note that in the case of discrete-time processes, if λ_t is weak-sense stationary and $E\left[\lambda_{t+\tau} | dn_t = 1\right]$ is independent of t, then dn_t is weak-sense stationary. This fact is shown in section A.4. Finally, the realization of a spike train from a doubly stochastic discrete-time point process with conditional intensity, λ_t, proceeds in the following way. At each time step, a realization of λ_t is

computed based on the previous history of the rate and spike process. A realization of dn_t is computed from a binary process with parameter $\Delta\lambda_t$. These values are then incorporated into the history to compute realizations for the subsequent time step. Note that for dn_t to be weak-sense stationary, the effect of initial conditions on the first two moments must vanish for sufficiently large t.

6.1 Spike Field Coherence. Let the centered increments of the discrete-time point process, dn_t be $d\tilde{n}_t$ such that,

$$d\tilde{n}_t = dn_t - E\,[dn_t]. \tag{6.3}$$

This ensures that $E\,[d\tilde{n}_t] = 0$, much like the x_t used in the development of the more standard random process employed in section 2 to define the field-field coherence, $C_{xy}(f)$. Then, in analogy withl equation 2.1, define the discrete Fourier transform of the centered increments, $d\tilde{n}_t$, as

$$N_T(f) = \frac{\Delta}{T} \sum_{t=0}^{N-1} e^{-i2\pi f t \Delta}\, d\tilde{n}_t, \tag{6.4}$$

where, as in equation (2.1), T is the duration of the time series and Δ is the sampling period. Let the local field potential recording be represented by the process y_t, introduced in section 2, with an associated discrete Fourier transform, $Y_T(f)$, defined in equation 2.2. Now, the coherence between the spiking and the local field potential, here after called the spike field coherence, $C_{\tilde{n}y}(f)$, is

$$C_{\tilde{n}y}(f) = \lim_{T\to\infty} \frac{E\left[N_T(f)Y_T^*(f)\right]}{\sqrt{E\left[\left|N_T(f)\right|^2\right] E\left[\left|Y_T(f)\right|^2\right]}}. \tag{6.5}$$

If the relevant spectra exist,

$$C_{\tilde{n}y}(f) = \frac{S_{\tilde{n}y}(f)}{\sqrt{S_{\tilde{n}\tilde{n}}(f)S_{yy}(f)}}, \tag{6.6}$$

where $S_{\tilde{n}y}(f)$ is the cross-spectrum between $d\tilde{n}_t$ and y_t, $S_{\tilde{n}\tilde{n}}(f)$ is the spectrum of $d\tilde{n}_t$, and $S_{yy}(f)$ is the spectrum of y_t. As in the discussion following equation 2.3, through the Cauchy-Schwartz inequality, $0 \leq \left|C_{\tilde{n}y}(f)\right| \leq 1$ and $\left|C_{\tilde{n}y}(f)\right| = 1$ when there is a linear relation between $N_T(f)$ and $Y_T(f)$. Note that the spike field coherence, $C_{\tilde{n}y}(f)$, differs from the field-field coherence, $C_{xy}(f)$, specified in equation 2.4, in that $S_{\tilde{n}y}(f)$ replaces $S_{xy}(f)$ in the

numerator of equation 2.4, and $S_{\tilde{n}\tilde{n}}(f)$ replaces $S_{xx}(f)$ in the denominator of equation 2.4.

The spike field cross-spectrum, $S_{\tilde{n}y}(f)$, can be related to an intensity-field cross-spectrum, $S_{\lambda y}(f)$, where λ denotes the intensity of the spiking process, dn_t. To show this, the spike field cross-spectrum is explicitly computed through use of the cross-covariance function, $r_{\tilde{n}y}(\tau)$, evaluated at lag τ. When the spectra are square integrable, a Fourier transform relation exists between the cross-spectra and the cross-covariance sequence of weak-sense stationary discrete-time random processes,

$$S_{\tilde{n}y}(f) = \Delta \sum_{\tau=-\infty}^{\infty} r_{\tilde{n}y}(\tau)e^{-i2\pi f\tau\Delta}. \tag{6.7}$$

In the following, note that the covariance functions, spectra, and coherences are the same between the centered and noncentered increments, dn_t. That is, $r_{\tilde{n}\tilde{n}}(t, \tau) = r_{nn}(t, \tau)$, and thus the spectra are equivalent, $S_{\tilde{n}\tilde{n}}(f) = S_{nn}(f)$, as are the coherences, $C_{\tilde{n}y}(f) = C_{ny}(f)$. This is due to the mean-removal operation present in the definitions of both the autocovariance and cross-covariance functions. In section A.2, we show that if the field, y_t, does not depend on past spikes, then

$$r_{ny}(\tau) = \Delta\, r_{\lambda y}(\tau), \tag{6.8}$$

where $r_{\lambda y}(\tau)$ is the intensity-field cross-covariance function evaluated at lag τ. Then, using equation 6.8 in equation 6.7, the spike field cross-spectrum is equal to the intensity field cross-spectrum scaled by the sampling period, Δ, that is,

$$S_{ny}(f) = \Delta\, S_{\lambda y}(f). \tag{6.9}$$

The spike-spike autocovariance function, $r_{\tilde{n}\tilde{n}}(t, \tau)$, is in general a function of two times: t, the global recording or observation time, and τ, the local lag relative to time t. In section A.3, we show that

$$r_{nn}(t, \tau) + \Delta^2 \mu_{\lambda,t}\, \mu_{\lambda,t+\tau}$$
$$= \begin{cases} \Delta\, \mu_{\lambda,t}, & \tau = 0 \\ \Delta^2\, E_{\lambda_t,\lambda_{t+\tau}}\left[\lambda_t\lambda_{t+\tau} \frac{P(\lambda_{t+\tau}|\lambda_t,dn_t=1)}{P(\lambda_{t+\tau}|\lambda_t)} \right], & |\tau| > 0 \end{cases}. \tag{6.10}$$

Here $\mu_{\lambda,t} = E\,[\lambda_t]$ is the expected intensity at time t, $P(\lambda_{t+\tau}|\lambda_t, dn_t = 1)$ is the probability density of the intensity at time $t + \tau$ given both the intensity at time, t, and the occurrence of a spike at time t. equation 6.10 describes a

history dependence within the expectation and, in general, nonstationary behavior. In section 6.1.1, equation 6.10, and the intimately related spike field coherence, $C_{ny}(f)$, specified in equation 6.6, are studied in the situation where the discrete time, doubly stochastic point process, dn_t, is Poisson, and in section 6.1.2, equation 6.10 is studied with the aid of a parametric model of the point process, dn_t.

6.1.1 Spike Field Coherence: Doubly Stochastic Poisson Process. As shown in section A.1, when dn_t is a doubly stochastic, discrete time Poisson process, $P(dn_t|\lambda_t, \lambda_{t+\tau}) = P(dn_t|\lambda_t)$. Then the ratio of probability density functions, $\frac{P(\lambda_{t+\tau}|\lambda_t, dn_t=1)}{P(\lambda_{t+\tau}|\lambda_t)}$, within the expecation in equation 6.10, is equal to 1 and the spike-spike autocovariance function, $r_{nn}(t, \tau)$, simplifies to

$$r_{nn}(t, \tau) = \begin{cases} \Delta\mu_{\lambda,t} - \Delta^2\mu_{\lambda,t}\mu_{\lambda,t+\tau}, & \tau = 0 \\ \Delta^2 r_{\lambda\lambda}(t, \tau), & |\tau| > 0 \end{cases}. \tag{6.11}$$

Here, $r_{\lambda\lambda}(t, \tau)$ is the autocovariance function of the stochastic intensity, λ_t. Further, when the stochastic intensity, λ_t, is weak-sense stationary, the spike-spike autocovariance does not depend on the global time, t, and the discrete time, doubly stochastic Poisson process, dn_t, becomes weak-sense stationary. Hence,

$$r_{nn}(\tau) = \begin{cases} \Delta\mu_\lambda - \Delta^2\mu_\lambda^2, & \tau = 0 \\ \Delta^2 r_{\lambda\lambda}(\tau), & |\tau| > 0 \end{cases}. \tag{6.12}$$

The separate behavior at $\tau = 0$ in equation 6.12 is not present for field-type weak-sense stationary discrete time random processes, such as y_t. The $\tau = 0$ case arises due to the fact that $E\left[dn_t^2\right] = E\left[dn_t\right]$. To see this, note that with the stipulation that the probability of multiple events in any one increment is vanishing small (see constraint 6.1 in section 2), dn_t for any fixed t is essentially a Bernoulli distributed random variable. Hence, dn_t takes on values 0 and 1. Since both 0 and 1 equal themselves when squared, the probability that dn_t equals 1 is equal to the probability of dn_t^2 equaling 1. Hence, $E\left[dn_t\right] = E\left[dn_t^2\right]$. Further, note that at $\tau = 0$, the autocovariance sequence, $r_{nn}(\tau)$, is orders of magnitude larger than at any other τ. For neuroscience data, Δ is typically around 10^{-3} seconds in duration, and hence the autocovariance sequence at τ equal to 0 is approximately three orders of magnitude larger than at $\tau \neq 0$.

The behavior of the autocovariance sequence of the discrete time doubly stochastic Poisson process modeling the spiking data at zero lag demonstrates a profound difference between field-field coherence and spike field coherence. Let $S_{\lambda\lambda}(f)$ be the spectrum of the stochastic intensity, λ_t. The spectrum of dn_t, assuming the existence and square integrability of the

spectrum, is

$$S_{nn}(f) = \Delta \sum_{\tau=-\infty}^{\infty} r_{nn}(\tau) e^{-i2\pi f \tau \Delta} \tag{6.13}$$

$$= \Delta^2 \left(\mu_\lambda + S_{\lambda\lambda}(f) \right) - \Delta^3 \left(r_{\lambda\lambda}(0) + \mu_\lambda^2 \right) \tag{6.14}$$

$$S_{nn}(f) \approx \Delta^2 \left(\mu_\lambda + S_{\lambda\lambda}(f) \right). \tag{6.15}$$

The units of μ_λ and of $S_{\lambda\lambda}(f)$ must be identical. Note that the units of $S_{\lambda\lambda}(f)$ are in Hz^2 per Hz, or Hz, as are the units of μ_λ. Further, note that the term neglected in the development of equation 6.15 is on the order of milliseconds, and hence, the approximation is valid up to an $O(10^{-3})$ correction for typical neuroscience time series. Though small, the importance of this neglected term will depend on required accuracy and on the sampling properties of available coherence estimators. Though not the focus of this letter, note that any bias resulting from the approximation in equation 6.15 will be of significance only if the estimator standard deviation can be held to a comparable level. For typical nonparametric spectrum estimators, the asymptotic standard deviation is $\sqrt{\frac{2}{\nu}} S(f)$, where $S(f)$ is the spectrum and ν is the estimator degrees of freedom. Typically ν does not exceed 20. From equation 6.15 one sees for $\Delta = 10^{-3}$ seconds, ν must exceed 10^6 before the typical estimator standard deviation nears the level where the approximate nature of equation 6.15 becomes apparent when analyzing data. Thus, for the remainder of this letter, equation 6.15 is considered to be exact.

With this expression for the spectrum of dn_t (see equation 6.15), combined with the spike field cross-spectrum (see equation 6.9), the spike field coherence (see equation 6.6) becomes

$$C_{ny}(f) = \frac{\Delta S_{\lambda y}(f)}{\sqrt{\Delta^2 \left(\mu_\lambda + S_{\lambda\lambda}(f) \right) S_{yy}(f)}} \tag{6.16}$$

$$= \frac{S_{\lambda y}(f)}{\sqrt{\left(\mu_\lambda + S_{\lambda\lambda}(f) \right) S_{yy}(f)}} \tag{6.17}$$

$$= C_{\lambda y}(f) \left(1 + \frac{\mu_\lambda}{S_{\lambda\lambda}(f)} \right)^{-\frac{1}{2}}. \tag{6.18}$$

Thus, the spike field coherence, $C_{ny}(f)$, when modeling the neuron spiking activity as a doubly stochastic discrete time Poisson process, depends on the mean intensity, μ_λ. More succinctly, given the model, the coherence depends on the overall activity of the neuron.

To further explore this dependence, consider scaling the intensity with the nonnegative constant, c, such that $\hat{\lambda}_t = c \lambda_t$. Because $\hat{\lambda}_t$ is the stochastic

intensity for the discrete time, doubly stochastic Poisson process, $d\hat{n}_t$, scaling the intensity affects the spiking that results. The scaled spike field cross-covariance, $r_{\hat{n}y}(\tau)$, becomes

$$r_{\hat{n}y}(\tau) = E\left[d\hat{n}_t y_{t+\tau}\right] - E\left[d\hat{n}_t\right] E\left[y_{t+\tau}\right]. \tag{6.19}$$

By conditioning, it can be shown that

$$r_{\hat{n}y}(\tau) = c\ \Delta\ E\left[\lambda_t y_{t+\tau}\right] - c\ \Delta\ E\left[\lambda_t\right] E\left[y_{t+\tau}\right] \tag{6.20}$$

$$= c\ r_{\tilde{n}y}(\tau). \tag{6.21}$$

Repeating the calculations leading to equation 6.15, with the intensity-scaled point process, $d\hat{n}_t$, yields the spike-field coherence, $C_{\hat{n}y}(c, f)$, as a function of the intensity scaling, c:

$$C_{\hat{n}y}(c, f) = \frac{c\ S_{\lambda y}(f)}{\sqrt{(c\mu_\lambda + c^2 S_{\lambda\lambda}(f))\ S_{yy}(f)}} \tag{6.22}$$

$$= \frac{S_{\lambda y}(f)}{\sqrt{\left(\frac{\mu_\lambda}{c} + S_{\lambda\lambda}(f)\right) S_{yy}(f)}}. \tag{6.23}$$

By taking the limit of $C_{\hat{n}y}(c, f)$ as c tends to 0 and as c tends to infinity, one can see how the spike field coherence, $C_{\tilde{n}y}(f)$, responds to changing mean intensity, or overall neuron activity, that is,

$$\lim_{c \to 0} C_{\hat{n}y}(c, f) = 0 \tag{6.24}$$

and

$$\lim_{c \to \infty} C_{\hat{n}y}(c, f) = C_{\lambda y}(f). \tag{6.25}$$

From equation 6.24, one sees that when there are no spikes, the spike field coherence is 0, and from equation 6.25, when the spiking activity becomes large, the spike field coherence equals the intensity field coherence, $C_{\lambda y}(f)$. For a simulation illustrating this behavior, see section 4; in particular, see Figure 1. This situation is in stark contrast with the effect of scaling either x_t or y_t on the field-field coherence, $C_{xy}(f)$, specified in equation 2.4. In the case of fields, scaling of x_t or y_t results in no change in $C_{xy}(f)$, as the effect of scaling on the numerator is cancelled by the effect of scaling on the denominator. In this sense, the behavior described in equation 6.24 and equation 6.25 is profound.

6.1.2 Spike Field Coherence: Doubly Stochastic Point Process. Actual spiking data exhibit a time-dependent probability of firing and dependence on past spiking events. This dependence often manifests in a refractory period or a period of bursting (Koch, 1999). Refraction is the phenomenon where there is a suppression of the probability of spiking immediately after a spiking event, and bursting is when immediately following a spiking event, the probability of spiking is temporarily increased. In either situation, the spike-spike autocovariance function, $r_{nn}(t, \tau)$ exhibits nonstationary behavior and depends in a complicated fashion on the probability density function of the intensity conditioned on past spiking events. This nonstationarity and dependence on historical spiking makes closed-form computations of the spectrum of dn_t through the transform of $r_{nn}(t, \tau)$ prohibitive. In this section, by introducing a parametric model for the spiking activity, dn_t, and making a high sampling-rate approximation, a simplification of equation 6.10 is attained, yielding an expression amenable to further analytic analysis.

Consider the following model for the stochastic intensity, λ_t, of dn_t, the doubly stochastic, history-dependent, discrete-time point process,

$$\lambda_t = g(x_t)\, e^{\sum_{j=1}^{J} a_j \lambda_{t-j} + \sum_{k=1}^{K} b_k dn_{t-k} + \epsilon_t}, \tag{6.26}$$

where the random innovation process, ϵ_t, satisfies $E[\epsilon_t] = 0$, $E[\epsilon_t \epsilon_{t'}] = \sigma_\epsilon^2 \delta_{t,t'}$, and the Kronecker delta function, $\delta_{t,t'}$, is 0 when $t \neq t'$ and is equal to 1 when $t = t'$. The function g of the covariate x_t is nonnegative and represents the dependence of the intensity (and therefore the spikes) on the field. The intensity, λ_t, also depends on the exponentiated autoregressive term, $\exp\left(\sum_{j=1}^{J} a_j \lambda_{t-j}\right)$, and the exponentiated linear combination of past spiking events, $\exp\left(\sum_{k=1}^{K} b_k dn_{t-k}\right)$, where the a_j and b_k are chosen such that $P(dn_t > 1) = O(\Delta_t^2)$. Because of these dependencies, this intensity model embodies complicated time-dependent spiking behavior and history dependence. Consequently, this model exhibits, at least qualitatively, salient features of actual neural spiking data.

Return to the spike-spike autocovariance, $r_{nn}(t, \tau)$, given in equation 6.10, and focus on the ratio of probability density functions within the expectation,

$$\frac{P(\lambda_{t+\tau}|\lambda_t, dn_t = 1)}{P(\lambda_{t+\tau}|\lambda_t)}. \tag{6.27}$$

In particular, consider three cases: $|\tau|$ is small relative to the refractory period τ_r, $|\tau|$ is comparable to the duration of the history effect due to a single spike and, τ is much larger than the duration of the history effect due to a single spike. When τ is greater than 0 and less than the refractory

period following a spike, $P(\lambda_{t+\tau}|\lambda_t, dn_t = 1)$ is a dirac-delta centered on 0, and the ratio of probability density functions, $\frac{P(\lambda_{t+\tau}|\lambda_t, dn_t=1)}{P(\lambda_{t+\tau}|\lambda_t)}$, is 0 for all $\lambda_{t+\tau}$ except when $\lambda_{t+\tau}$ is 0, where the ratio is infinite, and hence equation 6.10 is 0.

Next, for $\tau \gg K$, the effect of a spike at time t is reduced for physical models of neuron spiking, manifesting in history coefficients, b_τ, tending to 0 with increasing τ. That is, a spike at the current time has an effect on future intensities that diminish as time progresses. Hence, for $\tau \gg K$, the history coefficients $b_\tau \approx 0$ and the ratio of conditional densities, $\frac{P(\lambda_{t+\tau}|\lambda_t, dn_t=1)}{P(\lambda_{t+\tau}|\lambda_t)} = 1$. Note that when dn_t is weak-sense stationary, equation 6.10 is symmetric in τ. This result is developed in sections A.3 and A.4. Thus, for $|\tau| \gg K$, equation 6.27 equals

$$r_{nn}(t, \tau) = \Delta^2 r_{\lambda\lambda}(t, \tau), |\tau| \gg K. \tag{6.28}$$

When the stochastic intensity, λ_t is weak-sense stationary, $r_{\lambda\lambda}(t, \tau)$ does not depend on the global time, t, and

$$r_{nn}(\tau) = \Delta^2 r_{\lambda\lambda}(\tau), |\tau| \gg K,$$

such that the spike-spike autocovariance also does not depend on the global time, t. Then the discrete-time doubly stochastic point process, dn_t, is weak-sense stationary. In the final case, for intermediate values of $|\tau|$ in between these extreme values, the situation is more delicate and depends on the shape of the conditional densities. In the case where the stochastic intensity does not depend directly on past spiking, dn_t is Poisson, and the coefficients b_τ are 0 for all τ. In this situation, the probability densities within the expectation of equation 6.27 are identical, and the Poisson case discussed in section 6.1.1 is recovered. If there is limited history dependence, such that K in equation 6.26 is small, then the limit, $\tau \gg K$, is attained for relatively small $|\tau|$, and once again the Poisson situation discussed in section 6.1.1 is relevant. Let τ_o be the smallest positive lag at which the asymptotic ratio of conditional densities is approximately attained. Then, assuming a time-invariant expected intensity, the spike-spike autocovariance function, $r_{nn}(t, \tau)$, is

$$r_{nn}(t, \tau) = \begin{cases} \Delta\mu_\lambda - \Delta^2\mu_\lambda^2, & \tau = 0 \\ -\Delta^2\mu_\lambda^2, & 0 < |\tau| \leq \tau_r \\ \Delta^2 E\left[\lambda_t \lambda_{t+\tau} \frac{P(\lambda_{t+\tau}|\lambda_t, dn_t=1)}{P(\lambda_{t+\tau}|\lambda_t, dn_t=0)}\right] - \Delta^2\mu_\lambda^2, & \tau_r < |\tau| \leq \tau_o \\ \Delta^2 r_{\lambda\lambda}(\tau), & |\tau| > \tau_o \end{cases} \tag{6.29}$$

where the dependence on the global time t in equation 6.29 is limited to the case where $\tau_r < |\tau| < \tau_o$. As in the Poisson case, the spike-spike autocovariance, $r_{nn}(t, \tau)$, exhibits a dramatic change from $\tau = 0$ to $|\tau| > 0$, once again manifesting in a spike field coherence depending on the expected intensity. In equation 6.29, the value of the spike-spike autocovariance function for $\tau_r < |\tau| < \tau_o$ depends, in a possibly complicated fashion, on past values of dn_t, but this dependence is time limited to a duration of $\tau_o - \tau_r$. Hence, one expects the complicated history-dependent part of the spike-spike autocovariance function to contribute to the spectrum of dn_t through the convolution of a broad-band "smearing" function. This smearing reduces the effect of this term on the spike spectrum. To obtain an approximate expression, in analogy with equation 6.12 for the spike-spike autocovariance function when dn_t is doubly stochastic Poisson, postulate the existence of a nonnegative, symmetric function, $g(\tau)$, such that

$$g(\tau)E\left[\lambda_t\lambda_{t+\tau}\right] = E\left[\lambda_t\lambda_{t+\tau}\frac{P(\lambda_{t+\tau}|\lambda_t, dn_t = 1)}{P(\lambda_{t+\tau}|\lambda_t, dn_t = 0)}\right], \tau_r < |\tau| < \tau_o. \quad (6.30)$$

Then the lagged-product moment of the stochastic intensity is factored out of the expectation within equation 6.29. To facilitate discrete Fourier transformation, write the spike-spike autocovariance function in the following way,

$$r_{nn}(\tau) = \Delta^2 a(\tau) + \Delta\mu_\lambda\delta_\tau - \Delta^2\mu_\lambda^2, \quad (6.31)$$

where δ_τ is the Kronecker delta function, 0 for nonnegative τ, 1 when $\tau = 0$, and

$$a(\tau) = E[\lambda_t\lambda_{t+\tau}]\left\{1 - rect_{\tau_o}(\tau) + g(\tau)rect_{\tau_{ro}}\left(|\tau| - \frac{\tau_r + \tau_o}{2}\right)\right\}. \quad (6.32)$$

Here the rectangle function, $rect_\alpha(x)$, is

$$rect_\alpha(x) = \begin{cases} 1, & |x| \le \alpha \\ 0, & |x| > \alpha \end{cases}.$$

In section A.5, we show that the spectrum, $S_{nn}(f)$ of dn_t, equal to the discrete Fourier transform of the spike-spike autocovariance function, $r_{nn}(\tau)$, is equal to

$$S_{nn}(f) = S_{nn}^{(p)}(f) - \tilde{H}(f), \quad (6.33)$$

where $S_{nn}^{(p)}(f)$ is the spectrum of dn_t when dn_t is a discrete-time, doubly stochastic Poisson process,

$$S_{nn}^{(p)}(f) = \Delta^2 \big(S_{\lambda\lambda}(f) + \mu_\lambda \big), \qquad (6.34)$$

and the frequency-dependent correction term, $\tilde{H}(f)$, capturing the effect of history dependence on the spectrum of dn_t is

$$\tilde{H}(f) = \Delta^2 S_{\lambda\lambda}(f) * Q(f) + \Delta^3 \mu_\lambda^2 Q(f). \qquad (6.35)$$

Here $S_{\lambda\lambda}(f)$ is the spectrum of the stochastic intensity, λ_t. The convolving factor, $Q(f)$, is

$$Q(f) = G(f) * D_{\tau_{ro}}(f) - D_{\tau_r}(f), \qquad (6.36)$$

where $G(f)$ is the discrete Fourier transform of the unspecified $g(\tau)$, capturing the effect of history dependence on the spike-spike autocovariance function, $r_{nn}(\tau)$ for $\tau_r < |\tau| < \tau_o$, and $D_a(f)$ is the discrete Fourier transform of $rect_a(\tau)$. The half-width, τ_{ro}, is equal to $\frac{\tau_o - \tau_r}{2}$. When dn_t is a discrete-time, doubly stochastic Poisson process, $g(\tau) = 1$, the discrete Fourier transform of $g(\tau)$ is $G(f) = \delta(f)$, and there is no refractory period, such that $\tau_r = 0$. Then $Q(f) = 0$, and the correction term, $\tilde{H}(f)$, is 0. Hence the result from section 6.1.1 is recovered.

Because the correction, $\tilde{H}(f)$, to the Poisson spike-spike spectrum, $S_{nn}^{(p)}(f)$, required to obtain the spike-spike spectrum in the current situation depends predominantly on the function $Q(f)$, one sees that via the differencing operation between the Dirichlet-type kernels within $q(f)$, there is potential for a cancelling effect, tending to reduce the influence of history on the spike-spike spectrum. Finally, the spike field coherence, $C_{ny}(f)$, when dn_t is a discrete-time, doubly stochastic point process, as specified by equation 6.26, is, in analogy with equation 6.18,

$$C_{ny}(f) = C_{\lambda y}(f) \left(1 + \frac{\mu_\lambda - H(f)}{S_{\lambda\lambda}(f)} \right)^{-\frac{1}{2}}, \qquad (6.37)$$

where $H(f) = \Delta^{-2}\tilde{H}(f)$. Once again, the dependence of the spike field coherence, $C_{ny}(f)$, on the expected intensity, μ_λ, is explicit, and results analogous to the Poisson situation presented in section 6.1.1 hold.

The results of this section depend on the weak-sense stationary, doubly stochastic point-process class of models. The extent to which one can call the spike field coherence, $C_{ny}(f)$, defined in equation 6.18, the "true" spike field coherence depends on the extent to which a doubly stochastic weak-sense stationary, discrete-time point-process model accurately describes actual

spiking data and further the extent to which the model is robust to modeling inaccuracies.

7 Discussion

Within the confines of the doubly stochastic, weak-sense stationary discrete-time Poisson process model, we showed in section 6 that the theoretical spike field coherence, $C_{ny}(f)$, depends on the expectation of the stochastic rate, μ_λ. The dependence of the spike field coherence on the expected rate is a manifestation of the essentially Bernoulli nature of the increments of a discrete-time Poisson process with increments short with respect to the process rate. This dependence is not exhibited by the coherence between more standard models of time series, where the scaling of individual time series leaves the coherence unmodified.

In section 6.1.2 we showed, subject to an approximation, that the spike field coherence for a doubly stochastic, weak-sense stationary, discrete-time point process is dependent on the expected intensity in a fashion analogous with the situation where neuron activity is independent of past spiking. In this situation, history-dependence introduces an extra frequency and history-dependent correction term. This correction term reduces the ratio of the expected intensity to the intensity spectrum within the factor relating the intensity field coherence with the spike field coherence.

While the behavior of the spike field coherence detailed in section 6 depends on the weak-sense stationary doubly stochastic discrete-time point process model class, there is a sense in which this behavior can be a useful approximation to reality in the event of model misspecification. In particular, many instances exist where the weak-sense stationary assumption is made and successful inference performed (Brillinger, 2001; Percival & Walden, 1993; Priestly, 1981). Often this is accomplished by either recording over sufficiently short intervals such that this assumption is approximately true; by identifying short, weak-sense stationary sections of time in an otherwise nonstationary time series; or by noting how a spectral estimator will behave on a nonstationary time series and accounting for this behavior. On the other hand, there are instances where inference with nonstationary time series is best conducted by explicitly modeling the nonstationarity. Such efforts, with fieldtype time series, have led to the evolutionary spectrum, (see Priestly, 1965), and later work, and to the generalized, or Loève, spectrum, presented in, for example, Scharf & Friedlander (2001). Standard statistical procedure is to assess if nonstationary modeling is required and, accordingly, proceed with the appropriate inference. In the current context, that is, the analysis of spike field coherence, such methodology does not yet exist, and one might anticipate its development.

In short, this letter establishes the dependence of spike field coherence on expected intensity, or expected rate in the Poisson process situation, and establishes that this dependence on the overall neuron activity is a

population characteristic. The correct frequency-dependent measure of linear association between spiking data and nonspiking data depends on the total number of spikes that occur within a set interval of time.

In many situations, one is interested in the reliability of spiking at a specific phase of a narrow-band field rhythm. In this case, the desired quantity is the rate field coherence in the Poisson case and the intensity field coherence in the more general situation where history-dependent effects on spiking activity are present. This is justified as follows. The conditional intensity, when the probability of multiple spiking events in a single time step is negligible, is proportional to the probability of spiking. Thus, the intensity field coherence is a frequency-dependent measure of linear association between the probability of spiking and the field. When neuron firing reliably occurs at a specific phase of a rhythm, then the probability of firing is periodic in time with a timing commensurate with the phase of the field at which the neuron preferentially spikes. In this case, the coherence between the probability of spiking and the field is large, as a linear relation exists between the relevant frequency domain quantities. Thus, if one is interested in an association between the time at which a neuron fires in relation to the phase of a rhythm, irrespective of the overall neuron activity, then the desired quantity is the intensity field coherence, $C_{\lambda y}(f)$.

Though not the focus of this work, four potential avenues of inference are proposed. The first is documented in Gregoriou et al. (2009), where spikes are randomly removed to attain equal spike rates between comparative spike count time series. The second consists of identifying regimes where the spike field coherence approximates the intensity field coherence. For example, for firing rates exceeding some nominal value, it may be that the factor multiplying the intensity field coherence, $C_{\lambda y}(f)$ in equation 3.1 is approximately 1. In a third procedure, the intensity field coherence is directly estimated, and in a fourth inference method, the spiking data are directly modeled and inference conducted using the generalized linear model inferential procedure. The development of such approaches will be the focus of future work. New methods of characterizing associations between the spiking of individual units and large-scale neural rhythms will facilitate an improved understanding of neural representation and function.

Appendix

A.1 Doubly Stochastic Poisson Process. When dn_t is a doubly stochastic, discrete-time Poisson process, $P(dn_t|\lambda_t, \lambda_{t+\tau}) = P(dn_t|\lambda_t)$. This can be shown as follows. By definition,

$$P(dn_t, dn_{t+\tau}|\lambda_t, \lambda_{t+\tau}) = P(dn_t|\lambda_t)P(dn_{t+\tau}|\lambda_{t+\tau}). \tag{A.1}$$

The joint conditional density, $P(dn_t, dn_{t+\tau}|\lambda_t, \lambda_{t+\tau})$, can be expanded:

$$P(dn_t, dn_{t+\tau}|\lambda_t, \lambda_{t+\tau}) = P(dn_{t+\tau}|\lambda_t, \lambda_{t+\tau})P(dn_t|\lambda_t, \lambda_{t+\tau}), \tag{A.2}$$

$$= P(dn_{t+\tau}|\lambda_{t+\tau})P(dn_t|\lambda_t, \lambda_{t+\tau}). \tag{A.3}$$

Thus, $P(dn_t|\lambda_t, \lambda_{t+\tau}) = P(dn_t|\lambda_t)$.

A.2 Spike Field Autocovariance Sequence. In the following, the local field potential, modeled by y_t, is taken to be mean-zero and is approximated to be independent of any one spiking event, $dn_t = 1$, that is, $P(y_{t+\tau}|\lambda_t, dn_t = 1) \approx P(y_{t+\tau}|\lambda_t)$. This approximation is justified in that the local field potential is thought to arise from the combined spiking activity of a great many neurons. Hence, strong dependence on a spike from any one neuron is unlikely. Then,

$$r_{ny}(\tau) = r_{\tilde{n}y}(\tau) \tag{A.4}$$

$$= E\left[dn_t\, y_{t+\tau}\right] \tag{A.5}$$

$$= E_{\lambda_t, y_{t+\tau}}\left[\, y_{t+\tau}\, E\left[dn_t \mid y_{t+\tau}, \lambda_t\right]\right] \tag{A.6}$$

$$= E_{\lambda_t, y_{t+\tau}}\left[\, y_{t+\tau}\, P(dn_t = 1 \mid y_{t+\tau}, \lambda_t)\right] \tag{A.7}$$

$$= E_{\lambda_t, y_{t+\tau}}\left[\, y_{t+\tau}\, \frac{P(y_{t+\tau}|\lambda_t, dn_t = 1)}{P(y_{t+\tau}|\lambda_t)} P(dn_t = 1|\lambda_t)\right] \tag{A.8}$$

$$= E_{\lambda_t, y_{t+\tau}}\left[\, y_{t+\tau}\, \frac{P(y_{t+\tau}|\lambda_t, dn_t = 1)}{P(y_{t+\tau}|\lambda_t)} \Delta\lambda_t\right] \tag{A.9}$$

$$= \Delta\, E_{\lambda_t, y_{t+\tau}}\left[\, y_{t+\tau}\, \lambda_t\right] \tag{A.10}$$

$$= \Delta\, r_{\lambda y}(\tau). \tag{A.11}$$

A.3 Spike-Spike Autocovariance Sequence. The spike-spike autocovariance sequence, $r_{nn}(t, \tau)$, is,

$$r_{nn}(t, \tau) = r_{\tilde{n}\tilde{n}}(t, \tau), \tag{A.12}$$

$$= E\left[dn_t dn_{t+\tau}\right] - E\left[dn_t\right] E\left[dn_{t+\tau}\right]. \tag{A.13}$$

For a weak-sense stationary conditional intensity, λ_t, the expected value of the discrete time, doubly stochastic point process, dn_t is independent of time and equals, $\Delta\mu_\lambda$. Then,

$$r_{nn}(t, \tau) = E\left[dn_t dn_{t+\tau}\right] - \Delta^2\mu_\lambda^2. \tag{A.14}$$

Focusing on the first term on the right-hand side, the expectation of the lagged product of the spiking processes is

$$E\left[dn_t dn_{t+\tau}\right] = E_{\lambda_t, \lambda_{t+\tau}}\left[\, E\left[dn_t dn_{t+\tau} \mid \lambda_t, \lambda_{t+\tau}\right]\right]. \tag{A.15}$$

$$\tag{A.16}$$

For clarity, concentrate on the inner expectation in equation A.16, and consider the situation where $\tau > 0$. Then:

$$E\left[dn_t dn_{t+\tau} \mid \lambda_t, \lambda_{t+\tau}\right]$$

$$= E_{dn_t \mid \lambda_t, \lambda_{t+\tau}}\left[dn_t\, E\left[dn_{t+\tau} \mid \lambda_t, \lambda_{t+\tau}, dn_{t+\tau}\right]\right] \tag{A.17}$$

$$= E_{dn_t \mid \lambda_t, \lambda_{t+\tau}}\left[dn_t\, E\left[dn_{t+\tau} \mid \lambda_{t+\tau}\right]\right] \tag{A.18}$$

$$= \Delta\, E_{dn_t \mid \lambda_t, \lambda_{t+\tau}}\left[dn_t\, \lambda_{t+\tau}\right] \tag{A.19}$$

$$= \Delta\, \lambda_{t+\tau}\, P(dn_t = 1 \mid \lambda_t, \lambda_{t+\tau}), \tag{A.20}$$

$$= \Delta\, \lambda_{t+\tau}\, \frac{P(\lambda_{t+\tau} \mid \lambda_t, dn_t = 1)}{P(\lambda_{t+\tau} \mid \lambda_t)} P(dn_t = 1) \tag{A.21}$$

$$= \Delta^2\, \lambda_t \lambda_{t+\tau}\, \frac{P(\lambda_{t+\tau} \mid \lambda_t, dn_t = 1)}{P(\lambda_{t+\tau} \mid \lambda_t)}, \quad \tau > 0. \tag{A.22}$$

Here, in a slight abuse of notation, $P()$ denotes, when appropriate, either a probability mass function or a probability density function. When $\tau < 0$,

$$E\left[dn_t dn_{t+\tau} \mid \lambda_t, \lambda_{t+\tau}\right] = \Delta^2\, \lambda_t \lambda_{t+\tau}\, \frac{P(\lambda_t \mid \lambda_{t+\tau}, dn_t = 1)}{P(\lambda_t \mid \lambda_{t+\tau})}, \quad \tau < 0, \tag{A.23}$$

let $t + \tau = u$. Then

$$E\left[dn_{u+|\tau|} dn_u \mid \lambda_{u+|\tau|}, \lambda_u\right] = \Delta^2\, \lambda_{u+|\tau|} \lambda_u$$
$$\times \frac{P(\lambda_{u+|\tau|} \mid \lambda_u, dn_t = 1)}{P(\lambda_{u+|\tau|} \mid \lambda_u)}, \quad \tau < 0. \tag{A.24}$$

When λ_t satisfies condition (A.31), developed in section A.4, the density, $P(\lambda_{t+\tau} \mid \lambda_t, dn_t = q)$, for $q = 0, 1$ is independent of t. Thus,

$$E\left[dn_t dn_{t+\tau} \mid \lambda_t, \lambda_{t+\tau}\right] = \Delta^2\, \lambda_t \lambda_{t+\tau}$$
$$\times \frac{P(\lambda_t \mid \lambda_{t+\tau}, dn_t = 1)}{P(\lambda_t \mid \lambda_{t+\tau})}, \quad |\tau| > 0. \tag{A.25}$$

Finally, when $\tau = 0$, the autocovariance function, $r_{nn}(\tau)$, of the increments, dn_t, is

$$r_{nn}(t, \tau) = r_{\tilde{n}\tilde{n}}(t, \tau) \tag{A.26}$$

$$= E\left[dn_t^2\right] - \Delta^2 \mu_{\lambda,t}\, \mu_{\lambda,\tau} \tag{A.27}$$

$$= E\left[dn_t\right] - \Delta^2 \mu_{\lambda,t}\, \mu_{\lambda,\tau} \tag{A.28}$$

$$= \Delta \mu_{\lambda,t} - \Delta^2 \mu_{\lambda,t}\, \mu_{\lambda,\tau}. \tag{A.29}$$

Then,

$$
r_{nn}(t, \tau) + \Delta^2 \mu_{\lambda,t}\, \mu_{\lambda,t+\tau}
$$
$$
= \begin{cases} \Delta \mu_{\lambda,t}, & \tau = 0 \\ \Delta^2\, E_{\lambda_t,\lambda_{t+\tau}}\left[\,\lambda_t \lambda_{t+\tau}\, \frac{P(\lambda_{t+\tau}|\lambda_t, dn_t=1)}{P(\lambda_{t+\tau}|\lambda_t)}\,\right], & |\tau| > 0 \end{cases}. \tag{A.30}
$$

A.4 Doubly Stochastic Weak-Sense Stationarity.

Lemma 1. *Doubly-stochastic point-process, weak-sense stationary intensity: Let the stochastic intensity, λ_t, of the discrete-time doubly-stochastic discrete-time point process, dn_t be a weak-sense stationary discrete-time random process. In addition, if for any $t, t' \in \mathbb{Z}$,*

$$E\left[\lambda_{t+\tau} \mid dn_t = 1\right] = E\left[\lambda_{t'+\tau} \mid dn_{t'} = 1\right], \tag{A.31}$$

then dn_t is weak-sense stationary.

Proof. The proof follows by direct calculation. First, the mean of dn_t,

$$E\left[dn_t\right] = \Delta\, E\left[\lambda_t\right]. \tag{A.32}$$

Thus, if λ_t is weak-sense stationary, then $E\left[\lambda_t\right]$ is a constant independent of the absolute time, t. Therefore, $E\left[dn_t\right]$ is also a constant. It remains to show that the autocovariance sequence of dn_t does not depend on absolute time. The autocovariance sequence $r_{nn}(t, \tau)$, is

$$r_{nn}(t, \tau) = E\left[dn_t dn_{t+\tau}\right] - E\left[dn_t\right] E\left[dn_{t+\tau}\right]. \tag{A.33}$$

Focusing on the first term in equation A.33,

$$E\left[dn_t dn_{t+\tau}\right] = E_{dn_t}\left[\, dn_t\, E\left[dn_{t+\tau}|dn_t\right]\right] \tag{A.34}$$

$$= E\left[dn_{t+\tau}|dn_t = 1\right] P(dn_t = 1) \tag{A.35}$$

$$= \Delta E\left[\lambda_t\right] E\left[dn_{t+\tau}|dn_t = 1\right] \tag{A.36}$$

$$= \Delta E\left[\lambda_t\right] E_{\lambda_{t+\tau}|dn_t=1}\left[E\left[dn_{t+\tau}|\lambda_{t+\tau}, dn_t = 1\right]\right] \tag{A.37}$$

$$= \Delta E\left[\lambda_t\right] E_{\lambda_{t+\tau}|dn_t=1}\left[E\left[dn_{t+\tau}|\lambda_{t+\tau}\right]\right] \tag{A.38}$$

$$= \Delta E\left[\lambda_t\right] E_{\lambda_{t+\tau}|dn_t=1}\left[\Delta\lambda_{t+\tau}\right] \tag{A.39}$$

$$= \Delta^2 E\left[\lambda_t\right] E\left[\lambda_{t+\tau}|dn_t = 1\right]. \tag{A.40}$$

Then, an alternate expression, equivalent to equation A.30, for the spike-spike autocovariance, $r_{nn}(t, \tau)$, is,

$$r_{nn}(t, \tau) = \Delta^2 E\left[\lambda_t\right] E\left[\lambda_{t+\tau}|dn_t = 1\right] - \Delta^2 E\left[\lambda_t\right] E\left[\lambda_{t+\tau}\right]. \tag{A.41}$$

Thus, for dn_t to be weak-sense stationary, $E\left[\lambda_t\right]$ must be invariant with respect to changes in the time, t, as must $E\left[\lambda_{t+\tau}|dn_t = 1\right]$. Hence, weak-sense stationarity of the stochastic intensity, λ_t, along with the condition specified within equation A.31 of lemma 1 regarding the translation invariance of $E\left[\lambda_{t+\tau}|dn_t = 1\right]$, are conditions sufficient for lemma 1 to hold.

A.5 Spectrum of dn_t. Beginning with equation 6.31 for the spike-spike autocovariance function, $r_{nn}(\tau)$, use equation 6.15, essentially the discrete Fourier transform, to obtain the spectrum, $S_{nn}(f)$ of dn_t:

$$S_{nn}(f) = \Delta^3 \mathcal{F}(h(\tau)) + \Delta^2 \mu_\lambda - \Delta^3 \mu_\lambda^2 \mathcal{F}(1), \tag{A.42}$$

where $\mathcal{F}(x)$ denotes the discrete Fourier transform of x. Here, the discrete Fourier transform of 1, $\mathcal{F}(1)$ is equal to the dirac-delta function, $\delta(f)$, and

$$
\begin{aligned}
\mathcal{F}(h(\tau)) &= \mathcal{F}\left\{\left(r_{\lambda\lambda}(\tau) + \mu_\lambda^2\right)\left(1 - rect_{\tau_r}(\tau)\right.\right. \\
&\quad \left.\left. + g(\tau)\, rect_{\tau_{ro}}\left(|\tau| - \frac{\tau_r + \tau_o}{2}\right)\right)\right\} \\
&= \left\{\Delta^{-1} S_{\lambda\lambda}(f) + \mu_\lambda^2 \delta(f)\right\} \\
&\quad * \left\{\delta(f) - D_{\tau_r}(f) + \hat{g}(f) * D_{\tau_{ro}}(f)\right\},
\end{aligned} \tag{A.43}
$$

where $\mathcal{F}(g(\tau))$ is the discrete Fourier transform of $g(\tau)$, $D_{\tau_r}(f)$ is a Dirichlet-type kernel, equal to the discrete Fourier transform of $rect_{\tau_r}(\tau)$, and $D_{\tau_{ro}}(f)$ is the discrete Fourier transform of $rect_{\tau_{ro}}\left(|\tau| - \frac{\tau_r + \tau_o}{2}\right)$, that is,

$$D_{\tau_r}(f) = 2 \cos(\pi f \Delta \tau_r) \frac{sin(\pi f \Delta (\tau_r + 1))}{sin(\pi f \Delta)} - 1, \tag{A.44}$$

and, similarly, $D_{\tau_{ro}}(f)$,

$$\begin{aligned} D_{\tau_{ro}}(f) &= 2 \cos\left(\pi f \Delta (\tau_r + \tau_o)\right) \\ &\times \left(2 \cos(\pi f \Delta \tau_{ro}) \frac{sin(\pi f \Delta (\tau_{ro} + 1))}{sin(\pi f \Delta)} - 1\right), \end{aligned} \tag{A.45}$$

with $\tau_{ro} = \tau_o - \tau_r$. Let $q(f) = \hat{g}(f) * D_{\tau_{ro}}(f) - D_{\tau_r}(f)$, and combine equation A.42 with equation A.43 to obtain,

$$S_{nn}(f) = S_{nn}^{(p)}(f) - \tilde{H}(f), \tag{A.46}$$

where

$$S_{nn}^{(p)}(f) = \Delta^2 \left(S_{\lambda\lambda}(f) + \mu_\lambda\right), \tag{A.47}$$

and

$$\tilde{H}(f) = \Delta^2 S_{\lambda\lambda}(f) * q(f) + \Delta^3 \mu_\lambda^2 q(f). \tag{A.48}$$

A.6 Stationary Distribution of a Discrete Point Process. The model specified in equation 6.26 in section 6.1.2, while quite general, may not be weak-sense stationary. It is not clear that the model specified in equation 6.26 can, for some choice of parameters, be weak-sense stationary. To address this issue in some generality, lemma 2 is provided:

Lemma 2. *Stationary distribution of a discrete, doubly stochastic point process: Let $d\tilde{n}_t$ be a centered, finite-history, discrete-time, doubly-stochastic point process with a bounded number of events in any one interval. Then, in the limit as $t \to \infty$, $d\tilde{n}_t$ possesses a unique probability distribution independent of t.*

That is, reasonably behaved discrete-time doubly stochastic point processes are, for the purposes of statistical inference, stationary. Thus, lemma 2 allows a large class of models to be posited and analyzed as if they are stationary, without explicitly demonstrating this fact. Demonstrating model stationarity without appealing to lemma 2 can be nontrivial.

Proof. Heuristically, the steps to proving lemma 2 are the following:

1. Note that dn_t is a possibly large, but finite-order, Markov chain.
2. By augmenting the state-space of the Markov chain representation of dn_t, show that dn_t can be represented as a first-order Markov chain.
3. Show that the augmented first-order Markov chain representation of dn_t is aperiodic, irreducible, and positive recurrent.
4. From theorem 4.1 (Ross, 2009), note that an aperiodic, irreducible, first-order, positive recurrent Markov chain possesses, as $t \to \infty$, a unique, stationary distribution.

Step 1: Markov chain representation of dn_t. A Markov chain, x_t, of order, P, is a collection of random variables, where, conditioned on the P past random variables, a random variable, x_t, is independent of all other random variables occurring in the past:

$$P(x_t|x_{t-1},\ x_{t-2},\ \ldots,\ x_\infty) = P(x_t|x_{t-1},\ x_{t-2},\ \ldots, x_{t-P}). \tag{A.49}$$

Here, the state-space, that is, the values that x_t can assume, at any t, consists of numbers within the set of all integers: $x_t \in \mathbb{N}$. Note that dn_t takes on values in the integers, predominantly either 0 or 1, and has a history dependence that, though potentially infinite, is well approximated by finite-length history. Then,

$$P(dn_t|dn_{t-1},\ dn_{t-2},\ \ldots,\ dn_\infty) = P(dn_t|dn_{t-1},\ dn_{t-2},\ \ldots, dn_{t-M}),$$
$$\tag{A.50}$$

for some finite M.

Step 2: First-order markov chain representation of dn_t. Consider the augmentation of the state-space—the set of values that a Markov chain can represent at time t from scalar values to vector values. In particular, let $d\boldsymbol{n}_t$ be a Markov chain where, at any time, t,

$$d\boldsymbol{n}_t = \begin{pmatrix} dn_t \\ dn_{t-1} \\ \vdots \\ dn_{t-P} \end{pmatrix}, \tag{A.51}$$

where P is the possibly large but finite order of dn_t. Then,

$$P(d\boldsymbol{n}_t|\ d\boldsymbol{n}_{t-1},\ d\boldsymbol{n}_{t-2},\ \ldots)$$
$$= P(d\boldsymbol{n}_t|\ dn_{t-1},\ dn_{t-2},\ dn_{t-3},\ \ldots,\ dn_{t-P}, dn_{t-P-1},\ \ldots)$$
$$= P(d\boldsymbol{n}_t|\ dn_{t-1},\ dn_{t-2},\ dn_{t-3},\ \ldots,\ dn_{t-P})\ \ (\text{Markov-order } P \text{ property})$$
$$= P(d\boldsymbol{n}_t|\ d\boldsymbol{n}_{t-1}). \tag{A.52}$$

Hence, dn_t is an order 1 Markov chain.

Step 3 and 4: Aperiodicity, irreducibility and positive recurrence. The order 1 Markov chain, dn_t is aperiodic since if $dn_t = 0$, there is a nonzero probability of dn_t remaining in the same state at time $t + 1$. The Markov chain dn_t is irreducible since all states have a nonzero probability of being reached. And finally, dn_t is positive recurrent since the chain is irreducible and finite (Ross, 2009).

It is important to note that the refractory period makes the assumption of bounded state-space excellent. Similarly, while finite history dependence of dn_t is not strictly correct, a large but finite dependence on lagged dn_t is an acceptable approximation.

Acknowledgments

References

Amjad, A. M., Halliday, D. M., Rosenberg, J. R., & Conway, B. A. (1997). An extended difference of coherence test for comparing and combining several independent coherence estimates: Theory and application to the study of motor units and physiological tremor. *Journal of Neuroscience Methods, 73,* 69–79.

Bartlett, M. S. (1963). The spectral analysis of point processes. *Journal of the Royal Statistical Society, Series B (Methodological), 25*(2), 264–296.

Bartlett, M. S. (1981). *Introduction to stochastic processes: With special reference to methods and applications* (3rd ed.). Cambridge: Cambridge University Press.

Ben-Ari, Y. (2007). Physiologic and pathologic oscillations. *Trends in Neurosciences, 30*(7), 307–308.

Bollimunta, A., Chen, Y., Schroeder, C. E., & Ding, M. (2008). Neuronal mechanisms of cortical alpha oscillations in awake-behaving macaques. *J. Neurosci., 28*(40), 9976–9988. doi:10.1523/JNEUROSCI.2699-08.2008.

Brillinger, D. R. (2001). *Time series: Data analysis and theory.* Philadelphia: Society for Industrial and Applied Mathematics.

Brillinger, D., Lindsay, K. A., & Rosenberg, J. R. (2009). Combining frequency and time domain approaches to systems with multiple spike train input and output. *Biological Cybernetics, 100,* 459–474.

Bruns, A. (2004).   Fourier-, Hilbert- and wavelet-based signal analysis: Are they really different approaches?   *J. Neurosci. Methods, 137*(2), 321–322. doi:10.1016/j.jneumeth.2004.03.002.

Bruns, A., & Eckhorn, R. (2004). Task-related coupling from high- to low-frequency signals among visual cortical areas in human subdural recordings. *International Journal of Psychophysiology, 51*(2), 97–116.

Bullock, T. H., Mcclune, M. C., Achimowicz, J. Z., Iragui-Madoz, V. J., Duckrow, R. B., & Spencer, S. S. (1995). Temporal fluctuations in coherence of brain waves. *Proc. Natl. Acad. Sci. USA, 92*(25), 11568–11572.

Buzsaki, G., & Draguhn, A. (2004). Neuronal oscillations in cortical networks. *Science, 304*(5679), 1926–1929.

Buzsaki, G., Horváth, Z., Urioste, R., Hetke, J., & Wise, K. (1992).   High-frequency network oscillation in the hippocampus.   *Science, 256*(5059), 1025–1027.

Canolty, R. T., Edwards, E., Dalal, S. S., Soltani, M., Nagarajan, S. S., Kirsch, H. E., et al. (2006). High gamma power is phase-locked to theta oscillations in human neocortex. *Science, 313*(5793), 1626–1628.

Chalk, M., Herrero, J. L., Gieselmann, M. A., Delicato, L. S., Gotthardt, S., & Thiele, A. (2010). Attention reduces stimulus-driven gamma frequency oscillations and spike field coherence in v1. *Neuron, 66*(1), 114–125.

Chave, A. D., Thomson, D. J., & Ander, M. E. (1987). On the robust estimation of power spectra, coherences, and transfer functions. *Journal of Geophysical Research, 92*, 633–648.

Daley, D. J. & Vere-Jones, D. (2003). *An introduction to the theory of point processes*. Berlin: Springer.

DeCoteau, W. E., Thorn, C., Gibson, D. J., Courtemanche, R., Mitra, P., Kubota, Y., et al. (2007a). Learning-related coordination of striatal and hippocampal theta rhythms during acquisition of a procedural maze task. *Proc. Natl. Acad. Sci. USA, 104*(13), 5644–5649.

DeCoteau, W. E., Thorn, C., Gibson, D. J., Courtemanche, R., Mitra, P., Kubota, Y., et al. (2007b). Oscillations of local field potentials in the rat dorsal striatum during spontaneous and instructed behaviors. *Journal of Neurophysiology, 97*(5), 3800–3805.

Foster, M. R., & Guinzy, N. J. (1967). The coefficient of coherence: Its estimation and use in geophysical data processing. *Geophysics, 32*, 602.

Fries, P., Reynolds, J. H., Rorie, A. E., & Desimone, R. (2001). Modulation of oscillatory neuronal synchronization by selective visual attention. *Science, 291*(5508), 1560–1563.

Fries, P., Womelsdorf, T., Oostenveld, R., & Desimone, R. (2008). The effects of visual stimulation and selective visual attention on rhythmic neuronal synchronization in macaque area v4. *J. Neurosci., 28*(18), 4823–4835.

Gregoriou, G., Gotts, S. J., Zhou, H., & Desimone, R. (2009). High-frequency, long-range coupling between prefrontal and visual cortex during attention. *Science, 324*(5931), 1207–1210.

Halliday, D. M., Rosenberg, J. R., Amjad, A. M., Breeze, P., Conway, B. A., & Farmer, S. F. (1995). A framework for the analysis of mixed time series/point process data: Theory and application to the study of physiological tremor, single motor unit

discharges and electromyograms. *Progress in Biophysics and Molecular Biology, 64*, 237–278.

Hinich, M. J., & Clay, C. S. (1968). The application of the discrete Fourier transform in the estimation of power spectra, coherence, and bispectra of geophysical data. *Reviews of Geophysics, 6*(3), 347–363.

Jarvis, M., & Mitra, P. (2001). Sampling properties of the spectrum and coherency of sequences of action potentials. *Neural Computation, 13*(4), 717–749.

Jutras, M. J., Fries, P., & Buffalo, E. A. (2009). Gamma-band synchronization in the macaque hippocampus and memory formation. *J. Neurosci., 29*(40), 12521–12531.

Koch, C. (1999). *Biophysics of computation*. New York: Oxford University Press.

Kristeva, R., Patino, L., & Omlor, W. (2007). Beta-range cortical motor spectral power and corticomuscular coherence as a mechanism for effective corticospinal interaction during steady-state motor output. *Neuroimage, 36*(3), 785–792. doi:10.1016/j.neuroimage.2007.03.025.

Mandel, L., & Wolf, E. (1995). *Optical coherence and quantum optics*. Cambridge: Cambridge University Press.

Mitra, P., & Bokil, H. (2008). *Observed brain dynamics*. New York: Oxford University Press.

Montgomery, S. M., & Buzsáki, G. (2007). Gamma oscillations dynamically couple hippocampal CA3 and CA1 regions during memory task performance. *Proc. Natl. Acad. Sci. USA, 104*(36), 14495–14500.

Munk, W., & Phillips, N. (1968). Coherence and band structure of inertial motion in the sea. *Reviews of Geophysics, 6*(4), 447–476.

Nunez, P., Srinivasan, R., Westdorp, A., Wijesinghe, R., Tucker, D., Silberstein, R., et al. (1997). EEG coherency: I: Statistics, reference electrode, volume conduction, Laplacians, cortical imaging, and interpretation at multiple scales. *Electroencephalography and Clinical Neurophysiology, 103*(5), 499–515.

Oppenheim, A. V. & Schafer, R. W. (2009). *Discrete-time signal processing* (3rd ed.). Upper Saddle River, NJ: Prentice Hall.

Percival, D., & Walden, A. (1993). *Spectral analysis for physical applications*. Cambridge: Cambridge University Press.

Pereda, E., Quiroga, R., & Bhattacharya, J. (1995). Nonlinear multivariate analysis of neurophysiological signals. *Progress in Neurobiology, 77*, 1–37.

Pesaran, B., Nelson, M. J., & Andersen, R. A. (2008). Free choice activates a decision circuit between frontal and parietal cortex. *Nature, 453* (7193), 406–409.

Pesaran, B., Pezaris, J. S., Sahani, M., Mitra, P. P., & Andersen, R. A. (2002). Temporal structure in neuronal activity during working memory in macaque parietal cortex. *Nat. Neurosci., 5*(8), 805–811.

Priestly, M. B. (1965). Evolutionary spectra and non-stationary processes. *Journal of the Royal Statistical Society, Series B (Methodological), 27*(2), 204–237.

Priestly, M. B. (1981). *Spectral analysis and time series*. Orlando, Fl: Elsevier Academic Press.

Rosenberg, J. R., Halliday, D. M., Breeze, P., & Conway, B. A. (1998). Identification of patterns of neuronal connectivity: Partial spectra, partial coherence, and neuronal interactions. *Journal of Neuroscience Methods, 83*, 57–72.

Ross, S. M. (2009). *Introduction to probability models* (10th ed.). Orlando, FL: Academic Press.

Scharf, L. L., & Friedlander, B. (2001). Toeplitz and Hankel kernels for estimating time-varying spectra of discrete-time random processes. *IEEE Transactions on Signal Processing, 49*, 179–189.

Schmitt, J. M. (1999). Optical coherence tomography (OCT): A review. *IEEE Journal of Selected Topics in Quantum Electronics, 5*(4), 1205–1215.

Singer, W., & Gray, C. (1995). Visual feature integration and the temporal correlation hypothesis. *Ann. Rev. Neurosci., 18*, 555–586.

Sirota, A., Montgomery, S., Fujisawa, S., Isomura, Y., Zugaro, M., & Buzsáki, G. (2008). Entrainment of neocortical neurons and gamma oscillations by the hippocampal theta rhythm. *Neuron, 60*(4), 683–697.

Thomson, D. J. (1982). Spectrum estimation and harmonic analysis. *Proceedings of the IEEE, 70*, 1055–1096.

Towle, V. L., Carder, R. K., Khorasani, L., & Lindberg, D. (1999). Electrocorticographic coherence patterns. *Journal of Clinical Neurophysiology, 16*(6), 528–547.

Witham, C. L., Wang, M., & Baker, S. N. (2007). Cells in somatosensory areas show synchrony with beta oscillations in monkey motor cortex. *Eur. J. Neurosci., 26*(9), 2677–2686.

Womelsdorf, T., Fries, P., Mitra, P., & Desimone, R. (2006). Gamma-band synchronization in the visual cortex predicts speed of change detection. *Nature, 439*, 733–736.

Zaveri, H. P., Williams, W. J., Sackellares, J. C., Beydoun, A., Duckrow, R. B., & Spencer, S. S. (1999). Measuring the coherence of intracranial electroencephalograms. *Clinical Neurophysiology, 110*(10), 1717–1725.